Nanoscale

COMMUNICATION

View Article Online
View Journal | View Issue

Cite this: *Nanoscale*, 2014, **6**, 8575

Received 24th April 2014
Accepted 14th May 2014

DOI: 10.1039/c4nr02205j

www.rsc.org/nanoscale

Dirac fermion relaxation and energy loss rate near the Fermi surface in monolayer and multilayer graphene

C. W. Luo,*[a] P. S. Tseng,[a] H.-J. Chen,[a] K. H. Wu[a] and L. J. Li[b]

Ultrafast dynamics of Dirac fermions near the Fermi surface in monolayer and multilayer graphene are revealed using optical pump mid-infrared probe spectroscopy. The energy loss rate of Dirac fermions is also determined *via* energy-resolved transient transmissivity spectra, which is significantly suppressed as the number of layers in graphene increases.

Recently, 2D materials, such as graphene,[1] MoS_2, WS_2 and $MoSe_2$,[2] have become attractive because of their unique physical properties. Of these 2D materials, graphene is the simplest, composed of only a single element, carbon. Since the discovery of graphene by Novoselov and Geim,[1] many studies have demonstrated its unique properties of a high mobility of $\sim 2 \times 10^5$ cm^2 V^{-1} s^{-1} for both electrons and holes,[3] a high transmittance of ~97.7% in the visible range[4] and a high Young's modulus of ~1 TPa.[5] Different graphene-based devices have also been developed for various applications, such as FETs[6] and sensors.[7] Therefore, the issues associated with electron–phonon interaction, carrier lifetime, carrier dynamics and energy loss rate are very important for optimizing the device performance.

In 2008, Dawlaty *et al.*[8] first measured the ultrafast dynamics of photoexcited carriers in graphene using degenerate optical pump-probe spectroscopy. Similar measurements for mono- and multilayer epitaxial graphene have also been carried out by non-degenerate pump-probe spectroscopy, such as a dual-color optical pump probe,[9,10] an optical-pump infrared-probe,[11–13] an optical-pump THz-probe[14] and a THz-pump optical-probe.[15] However, the Dirac fermion–phonon coupling or energy loss rate in the vicinity of the Fermi level has not been studied. In this study, graphene is pumped by 800 nm and probed with a tunable mid-infrared to determine the Dirac fermion–phonon coupling and energy loss rate near the Fermi level.

The graphene samples were synthesized using CVD on a copper substrate. By carefully controlling the airflow of a mixture of methane and hydrogen in a heated furnace, monolayer graphene was uniformly grown on a copper substrate. The samples were then spin coated with poly(methyl methacrylate) (PMMA). PMMA/graphene was detached from the copper substrate by etching copper with an aqueous nitric acid solution. The detached PMMA/graphene was then transferred and deposited on the sapphire substrate by direct contact. PMMA was subsequently dissolved, leaving monolayer graphene on the target substrate. PMMA residues on the sample were then eliminated by annealing. *N*-layer graphene samples were obtained by repeating this process with *N* times on the same sapphire substrate. In this study, p-type graphene samples were used on the sapphire substrate, with $N = 1$, 2, 3 and 5, respectively. The number of layers in each sample was confirmed by the quantized absorption level for each sample, as noted in the optical transmission measurement using broadband visible light.

For optical pump mid-infrared probe (OPMP) spectroscopy,[16] the light source was provided by a regenerative amplifier (Legend, Coherent Inc.) operating at a central wavelength of 800 nm, with a repetition rate of 5 kHz, a spectral width of 35 nm and a pulse duration of 30 fs. A beam splitter reflected 40% of the light into the pump path, with the remainder being transmitted to serve as a probe. In the probe path, a 0.7 mm thick GaSe crystal generated mid-infrared (MIR) pulses with tunable wavelengths from 9.0 (138 meV) to 14.1 μm (88 meV) *via* differential frequency generation (DFG). In order to ensure the spot size of the pump beam was larger than that of the probe beam, the optical pump beam was focused on the sample to provide a spot with a diameter of 485 μm, using a 150 mm lens. The typical pumping fluence used in this study was 68 μJ cm^{-2}. The mid-infrared probe beam was focused on the sample surface to produce a spot with a diameter of 392 μm through an Au coated off-axis parabolic mirror with $f = 200$ mm. This beam was collimated and refocused onto a liquid-nitrogen cooled HgCdTe detector using an Au coated off-axis parabolic mirror with a focal length of 50 mm.

[a]*Department of Electrophysics, National Chiao Tung University, Hsinchu 30010, Taiwan. E-mail: cwluo@mail.nctu.edu.tw*

[b]*Institute of Atomic and Molecular Sciences, Academia Sinica, Taipei 10617, Taiwan*

Fig. 1 shows the optical pump mid-infrared probe spectra for all of the samples in this study. At low probe photon energy (E_p), a negative peak is clearly observed in the transient transmissivity changes, $\Delta T/T$. This negative peak gradually diminishes as the probe photon energy increases (in Fig. 1(a)). Noticeably, an additional positive peak appears at a greater probe photon energy of $E_p > 126$ meV, which is close to the Fermi energy, E_F (here, we take the Dirac point energy, E_D, to be zero). In order to elucidate the origins of both positive and negative signals, a model for the optical pumping and mid-infrared probing processes in the schematic energy band structure of the graphene is shown in Fig. 1(b). Since the photon energy of the MIR probe pulse ranges from 88 to 138 meV, the interband transitions between the valence band (VB) and the conduction band (CB) in the vicinity of the Fermi surface of graphene can be clearly observed. After pumping, the smearing effect causes the transient occupation probability above (below) E_F is to be larger (smaller) than that before pumping. Therefore, $\Delta T/T$ induced by the pump pulses is positive (negative) for the probe transitions above (below) E_F, which is consistent with the results for n-type graphene.[11]

This phenomenon is also demonstrated by the transient spectra, as shown in Fig. 2(a). For monolayer graphene, $\Delta T/T$ at 1.0 ps changes from negative to positive and crosses zero at around 132 meV. After 1.0 ps, the transient spectra gradually shrink with increasing delay time. Similar results are also observed for samples with two, three and five layers, as shown in Fig. 2(b)–(d). The variation in the transient spectra at 1.0 ps increases when the number of layers is increased. Additionally, the zero crossing point gradually shifts to the lower probe photon energy as the number of layers increases, which indicates that the Fermi surface is moving away from the Dirac point. The inset in Fig. 2 further presents the dependence of E_F on the number of layers in graphene. E_F linearly decreases as the number of layers increases, which is consistent with the results in ref. 11 and 17, in which the graphene samples were prepared by thermal desorption on SiC substrates. It is worth emphasizing that the Fermi level of graphene produced using CVD in this study is smaller than that of those produced by thermal desorption on SiC substrates.[11,17] This indicates that graphene grown by CVD has a smaller doping effect from substrates and is close to the intrinsic graphene.

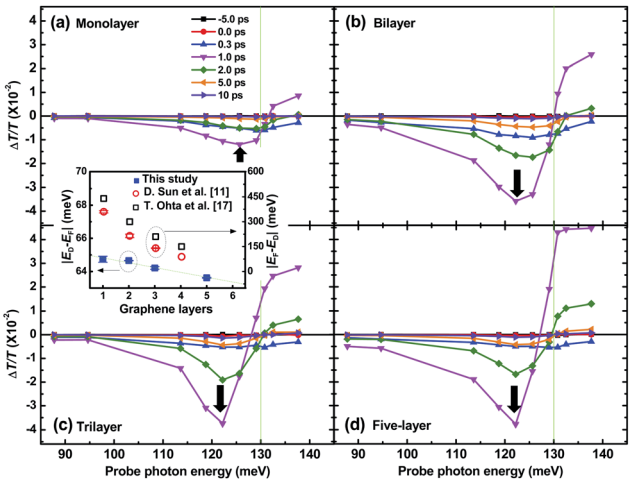

Fig. 2 The transient spectra at different delay times for the graphene samples with (a) monolayer, (b) bilayer, (c) trilayer and (d) five-layer. Inset: the energy difference between the Fermi level (E_F) and the Dirac point (E_D) as a function of the number of graphene layers.

The decay time (τ) of $\Delta T/T$ above E_F significantly depends on the probing photon energy, as shown in Fig. 3(a). For monolayer graphene, τ is larger and remains constant at ~2 ps when the probed regime is closer to E_F. A similar energy dependence of τ is also observed in multilayer graphene (bilayer, trilayer and five-layer). However, all of the τ values for multilayer graphene are larger than those for monolayer graphene, because the cooling of photoexcited hot carriers in multilayer graphene is slower than that in monolayer graphene. Additionally, the slope of $\tau(E)$ in the range of >5 meV is also larger than that for multilayer graphene. This implies that the smearing effect around E_F induced by optical pumping is significant in monolayer graphene.

Phonons are thought to be the main medium for the relaxation of photoexcited hot carriers in graphene.[9,11,12,14] Here, we follow this approach. The dependence of the relaxation time on the photon energy implies that the coupling strength (λ) between Dirac fermions and phonons varies at different positions on the Dirac cone. According to the second moment of the Eliashberg function,[18] λ is inversely proportional to the relaxation time (τ) of excited electrons,

$$\lambda\langle\omega^2\rangle \propto \frac{1}{\tau} \quad (1)$$

where ω is the phonon energy, which couples with the electrons. For the estimate of $\langle\omega^2\rangle$, some vibrational modes are more efficiently coupled to Dirac fermions than others are. In the case of graphene, the E_{2g} mode (which is the so-called G peak in the Raman spectra) of ~195.9 meV is coherently excited by photoexcitation and efficiently coupled.[19] After pumping, the temperature of the electrons (T_e) suddenly rises due to the smaller coefficient of heat capacity. Taking T_e = 2162 K (obtained from ref. 20 at the pumping fluence, as mentioned

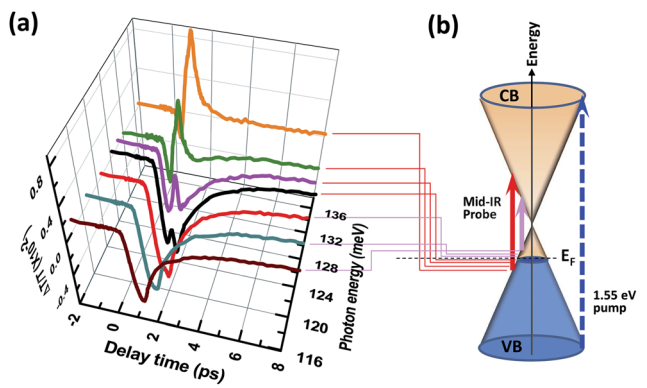

Fig. 1 (a) $\Delta T/T$ for monolayer graphene at various photon energies, from 88 to 138 meV. (b) The schematic energy band structure of graphene with the optical pump mid-IR probe processes.

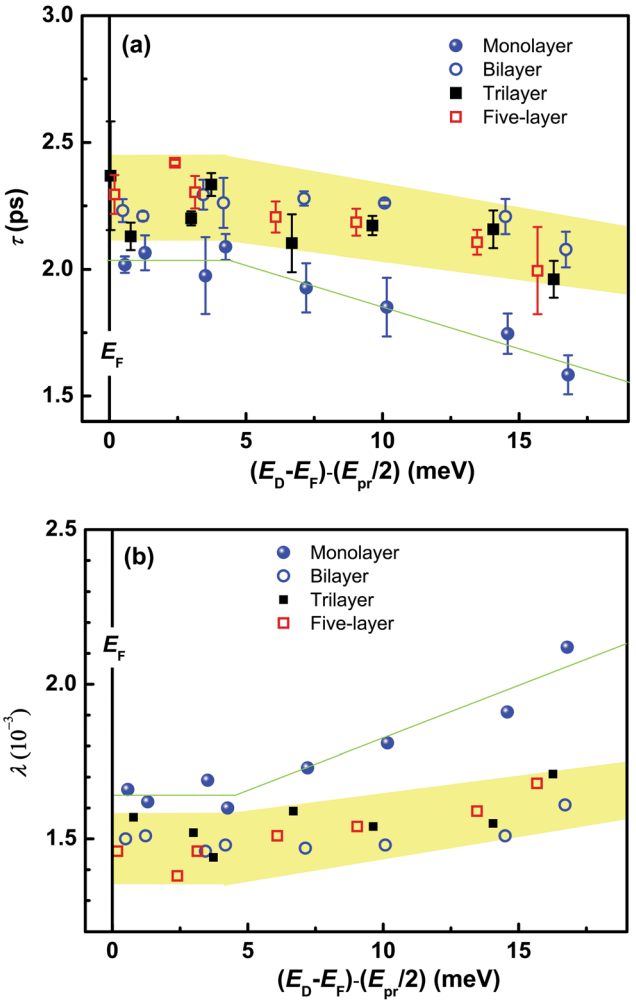

Fig. 3 The relaxation time for Dirac fermions as a function of the distance from the Fermi surface (E_F) for various graphene samples with monolayer, bilayer, trilayer and five-layer. (b) The Dirac fermion–phonon coupling constant as a function of the distance from the Fermi surface (E_F) for various graphene samples with monolayer, bilayer, trilayer and five-layer. The solid lines and gray areas are a guide for the eyes.

previously) to estimate the coefficient of $(\pi k_B T_e/3\hbar)$ in eqn (1), the photon energy dependence of the Dirac fermion–phonon coupling strength λ is shown in Fig. 3(b). The Dirac fermion–phonon coupling strength, measured using OPMP, becomes significantly smaller near E_F, which is in close agreement with the theoretical results of $\lambda \sim 3 \times 10^{-3}$,[21] obtained by using a continuum model to calculate the self-energy of phonon Green's function in graphene.

Fig. 3(b) shows the λ value for graphene as a function of the energy difference above E_F. For multilayer graphene (including two, three and five layers), the value of λ is around 1.5×10^{-3} below 5 meV and then slightly increases above 5 meV. Similar results are also observed in monolayer graphene. However, the value of $\lambda \sim 1.65 \times 10^{-3}$ is higher than that of multilayer graphene below 5 meV and rises much significantly to close to the theoretical value of 3×10^{-3} as the energy increases above 5 meV.[21] These results demonstrate that the Dirac fermion–phonon coupling strength above the Fermi level in monolayer graphene is higher than that in multilayer graphene. Moreover, the Dirac fermion–phonon coupling strength in monolayer graphene exhibits marked energy dependence above the Fermi level.

Finally, a closer examination of $\Delta T/T$ as a function of photon energy at various delays in Fig. 2 reveals that the absorption peak (marked by arrows in Fig. 2) experiences a red shift (relative to the zero crossing point, E_F) with the time delay. This implies the unoccupied density of states in the Dirac cone shift as a function of time, *i.e.*, the energy loss of carriers as a function of time. According to the first moment,

$$\left(\int \frac{\Delta T}{T} E_{\text{photon}} \mathrm{d}E_{\text{photon}}\right) \Big/ \left(\int \frac{\Delta T}{T} \mathrm{d}E_{\text{photon}}\right) \quad (2)$$

the rate of energy loss for the carriers in the Dirac cone is estimated. As shown in Fig. 4, the dots represent the first moment at a different time, which is associated with the red shift in the absorption peak shown in Fig. 2. An exponential fit to the time-dependent first moment shown in Fig. 4 gives a relaxation time of 0.35 ps within the range of 6.2 meV in monolayer graphene. Therefore, the rate of energy loss for Dirac fermions in the Dirac cone of monolayer graphene is ~17.7 meV ps^{-1}, which is much larger than that of 1 meV ps^{-1} in topological insulators.[16,22] For bilayer, trilayer and five-layer graphene, the rate of energy loss for Dirac fermions in the Dirac cone is 16.8, 8.6 and 3.8 meV ps^{-1}, respectively. This demonstrates that the number of layers in graphene is an important parameter for control of the energy loss rate, which is

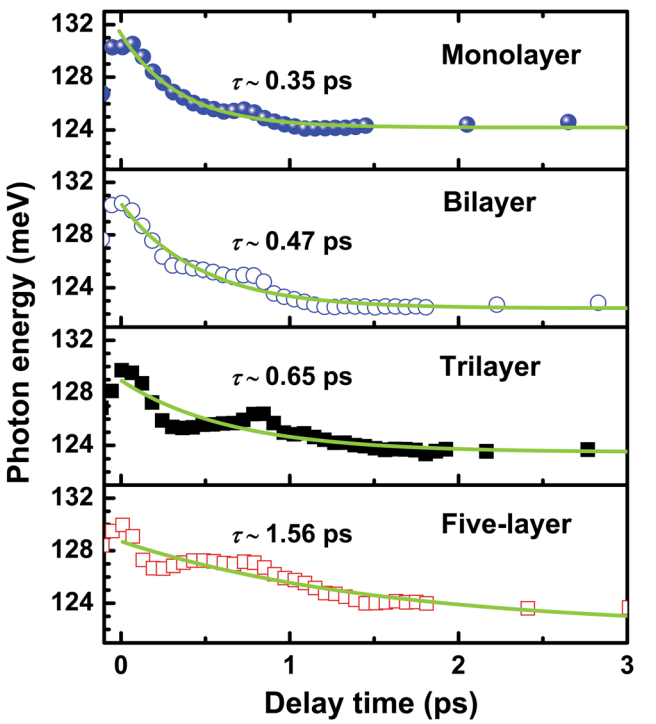

Fig. 4 The time-dependent first moment as a function of the delay time for various graphene samples with monolayer, bilayer, trilayer and five-layer. The solid lines are the exponential fitting curves.

significantly decreased when the number of layers increases. Consequently, this parameter, measured by OPMP, is extremely important for optoelectronic design, especially in the IR and THz range.

Conclusions

The Dirac fermion ultrafast dynamics in the vicinity of the Fermi surface in monolayer and multilayer graphene are studied using optical pump mid-infrared probe spectroscopy. The Fermi level of graphene with different numbers of layers is clearly identified by the change of sign of $\Delta T/T$. From the probe energy-dependent relaxation time, the Dirac fermion–phonon coupling strength is obtained as a function of energy near the Fermi surface using the two-temperature model. Additionally, the energy-resolved transient transmissivity spectra disclose that the rate of energy loss for Dirac fermions at room temperature is strongly dependent on the number of layers and it is significantly reduced as the number of layers in graphene increases.

Acknowledgements

This work was supported by the Ministry of Science and Technology, Taiwan, Republic of China (Contract no. 101-2112-M-009-016-MY2, 103-2923-M-009-001-MY3, and 102-2112-M-009-006-MY3), the Grant MOE ATU Program at NCTU.

Notes and references

1 K. S. Novoselov, A. K. Geim, S. V. Morozov, D. Jiang, M. I. Katsnelson, I. V. Grigorieva and S. V. Dubonos, *Nature*, 2005, **438**, 197.
2 J. N. Coleman, M. Lotya, A. O'Neill, S. D. Bergin, P. J. King, U. Khan, K. Young, A. Gaucher, S. De, R. J. Smith, I. V. Shvets, S. K. Arora, G. Stanton, H.-Y. Kim, K. Lee, G. T. Kim, G. S. Duesberg, T. Hallam, J. J. Boland, J. J. Wang, J. F. Donegan, J. C. Grunlan, G. Moriarty, A. Shmeliov, R. J. Nicholls, J. M. Perkins, E. M. Grieveson, K. Theuwissen, D. W. McComb, P. D. Nellist and V. Nicolosi, *Science*, 2011, **331**, 568.
3 S. V. Morozov, K. S. Novoselov, M. I. Katsnelson, F. Schedin, D. C. Elias, J. A. Jaszczak and A. K. Geim, *Phys. Rev. Lett.*, 2008, **100**, 016602.
4 R. R. Nair, P. Blake, A. N. Grigorenko, K. S. Novoselov, T. J. Booth, T. Stauber, N. M. R. Peres and A. K. Geim, *Science*, 2008, **320**, 1308.
5 C. Lee, X. Wei, J. W. Kysar and J. Hone, *Science*, 2008, **321**, 385.
6 Y.-M. Lin, C. Dimitrakopoulos, K. A. Jenkins, D. B. Farmer, H.-Y. Chiu, A. Grill and P. Avouris, *Science*, 2010, **327**, 662.
7 Y. Zhang, T. Liu, B. Meng, X. Li, G. Liang, X. Hu and Q. J. Wang, *Nat. Commun.*, 2013, **4**, 1811.
8 J. M. Dawlaty, S. Shivaraman, M. Chandrashekhar, F. Rana and M. G. Spencer, *Appl. Phys. Lett.*, 2008, **92**, 042116.
9 L. Huang, G. V. Hartland, L.-Q. Chu, Luxmi, R. M. Feenstra, C. Lian, K. Tahy and H. Xing, *Nano Lett.*, 2010, **10**, 1308.
10 K. M. Dani, J. Lee, R. Sharma, A. D. Mohite, C. M. Galande, P. M. Ajayan, A. M. Dattelbaum, H. Htoon, A. J. Taylor and R. P. Prasankumar, *Phys. Rev. B: Condens. Matter Mater. Phys.*, 2012, **86**, 125403.
11 D. Sun, C. Divin, C. Berger, W. A. de Heer, P. N. First and T. B. Norris, *Phys. Rev. Lett.*, 2010, **104**, 136802.
12 S. Winnerl, M. Orlita, P. Plochocka, P. Kossacki, M. Potemski, T. Winzer, E. Malic, A. Knorr, M. Sprinkle, C. Berger, W. A. de Heer, H. Schneider and M. Helm, *Phys. Rev. Lett.*, 2011, **107**, 237401.
13 T. Limmer, J. Feldmann and E. D. Como, *Phys. Rev. Lett.*, 2013, **110**, 217406.
14 P. A. George, J. Strait, J. Dawlaty, S. Shivaraman, M. Chandrashekhar, F. Rana and M. G. Spencer, *Nano Lett.*, 2008, **8**, 4248.
15 S. Tani, F. Blanchard and K. Tanaka, *Phys. Rev. Lett.*, 2012, **109**, 166603.
16 C. W. Luo, H. J. Wang, S. A. Ku, H.-J. Chen, T. T. Yeh, J.-Y. Lin, K. H. Wu, J. Y. Juang, B. L. Young, T. Kobayashi, C.-M. Cheng, C.-H. Chen, K.-D. Tsuei, R. Sankar, F. C. Chou, K. A. Kokh, O. E. Tereshchenko, E. V. Chulkov, Y. M. Andreev and G. D. Gu, *Nano Lett.*, 2013, **13**, 5797.
17 T. Ohta, A. Bostwick, J. L. McChesney, T. Seyller, K. Horn and E. Rotenberg, *Phys. Rev. Lett.*, 2007, **98**, 206802.
18 P. B. Allen, *Phys. Rev. Lett.*, 1987, **59**, 1460.
19 S. Reich and C. Thomsen, *Philos. Trans. R. Soc., A*, 2004, **362**, 2271.
20 J. C. Johannsen, S. Ulstrup, F. Cilento, A. Crepaldi, M. Zacchigna, C. Cacho, I. C. Edmond Turcu, E. Springate, F. Fromm, C. Raidel, T. Seyller, F. Parmigiani, M. Grioni and P. Hofmann, *Phys. Rev. Lett.*, 2013, **111**, 027403.
21 T. Ando, *J. Phys. Soc. Jpn.*, 2006, **75**, 124701.
22 C. W. Luo, H.-J. Chen, C. M. Tu, C. C. Lee, S. A. Ku, W. Y. Tzeng, T. T. Yeh, M. C. Chiang, H. J. Wang, W. C. Chu, J.-Y. Lin, K. H. Wu, J. Y. Juang, T. Kobayashi, C.-M. Cheng, C.-H. Chen, K.-D. Tsuei, H. Berger, R. Sankar, F. C. Chou and H. D. Yang, *Adv. Optical Mater.*, 2013, **1**, 804.

